MAVEN-STATIC observations of ion temperature and initial ion acceleration in the Martian ionosphere

K.G. Hanley[1*], C. M. Fowler[2], J. P. McFadden[1], D. L. Mitchell[1], S. Curry[1]

[1]Space Sciences Laboratory, University of California Berkeley, 7 Gauss Way, Berkeley, CA 94720
[2]Department of Physics and Astronomy, West Virginia University, Morgantown, West Virginia 26506

Key Points:

- Ion temperature profiles calculated from MAVEN STATIC data are presented as a function of SZA and altitude in the Mars ionosphere
- Suprathermal components appear in ion distribution functions starting just above the exobase region at all SZAs
- Crustal magnetic fields appear to reduce low-altitude energization of planetary plasma on the dayside and enhance it on the nightside

*Space Sciences Laboratory, University of California Berkeley, 7 Gauss Way, Berkeley, CA 94720

Corresponding author: K. Gwen Hanley, gwen.hanley@berkeley.edu

Abstract

Though ion escape to space is an important mechanism for atmospheric loss on Mars, the processes that accelerate ions to escape velocity have not been fully identified and quantified. The lowest altitude where suprathermal planetary ions appear is an important source region for ion escape, where electromagnetic forces and waves begin to energize ions to escape velocity. We have conducted a statistical study of O_2^+ distribution functions measured by Mars Atmosphere and Volatile EvolutioN SupraThermal And Thermal Ion Composition (MAVEN-STATIC) in order to identify the region where suprathermal tails appear. At all solar zenith angles, suprathermal ions appear just above the exobase region, where the mean free path between collisions exceeds the neutral gas scale height. O_2^+ temperature profiles are also presented. We also investigate the effects of crustal magnetism, finding that crustal fields protect planetary plasma on the dayside and enhance energization on the nightside.

1 Introduction

Mars has lost most of its atmosphere through escape to space, which has played a critical role in the planet's climate evolution (Jakosky et al., 2018). Although most atmospheric neutrals are cold and heavy, so that Jeans escape is negligible, photochemistry in the thermosphere produces some hot neutral species that can escape in appreciable quantities (Fox & Hać, 2009; Chaffin et al., 2017; Lillis et al., 2017). In the current epoch, this photochemical escape is the dominant loss process, but observations have shown that ion escape could account for as much as 30% of the total loss (Lundin et al., 1989; Jakosky et al., 2018; Ramstad et al., 2018). However, ions are created from the neutral atmosphere through photoionization or impact ionization, typically at energies far below the energy needed to escape the planet's gravity (Schunk & Nagy, 2009). The processes through which planetary ions are accelerated to escape energy at Mars (4.2 eV for O_2^+) have not yet been fully identified and quantified.

Some steps in the process of ion acceleration are understood. Because the major source of ions is ultimately the cold neutral atmosphere (∼200 K in the dayside ionosphere (Stone et al., 2018)), Jeans escape of the highest energy ions can remove only a small fraction of the gravitationally bound thermal ion population. The ambipolar electric field, generated by the difference in thermal velocities of ions and electrons, accelerates ions upward and provides a boost to Jeans escape (Ergun et al., 2016). The total potential drop due to the ambipolar field in Mars' ionosphere has been estimated to be <1.5 V (Xu et al., 2018; Akbari et al., 2019), not enough to accelerate most ions to escape energy. In addition to the acceleration by the ambipolar field, electromagnetic waves heat ions above the exobase region (Ergun et al., 2006). Case studies have shown that wave heating can lead to the development of suprathermal tails in ion distributions at Mars (e.g. Collinson et al., 2018; Fowler et al., 2018, 2021). However, the processes that form these suprathermal tails and their importance for ion escape are not yet fully understood.

This paper is the first step in comprehensively addressing the problem of suprathermal tail formation by determining in statistical fashion where suprathermal ion populations are observed in data collected by the Mars Atmosphere and Volatile EvolutioN (MAVEN) mission (Jakosky et al., 2015). We also present ion temperature profiles as a function of solar zenith angle (SZA) and altitude between 150 km and 500 km. Finally, we discuss variations in ion temperature and energization with changing SZA and altitude, and the effects of crustal magnetism.

2 Method & Observations

2.1 Data

Data used in this study were collected by MAVEN's SupraThermal And Thermal Ion Composition (STATIC) instrument (McFadden et al., 2015), a toroidal top-hat electrostatic analyzer with attached time-of-flight velocity analyzer. STATIC is capable of distinguishing Mars' main ionospheric and escaping species (H^+, H_2^+, He^+, C^+, O^+, O_2^+ and CO_2^+) with a field-of-view (FOV) covering 360°x90°. The energy and angular widths of measured O_2^+ velocity distribution functions are used to determine O_2^+ temperature using the method described by Hanley et al. (2021), which assumes the ions have a dominant Maxwellian component. Distribution functions and temperatures are sampled every 4 seconds and are corrected for spacecraft potential, instrument response, internal scattering, and a time-varying detuning of the electrostatic analyzer referred to as "ion suppression." Data used in this paper were measured during more than 10,400 MAVEN orbits ranging from February 2016 to December 2020. MAVEN's precessing elliptical orbit allows periapsis to sample the full range of SZA, local time, and longitude for latitudes equatorward of 75°. We have binned the data into 25 km altitude bins and SZA

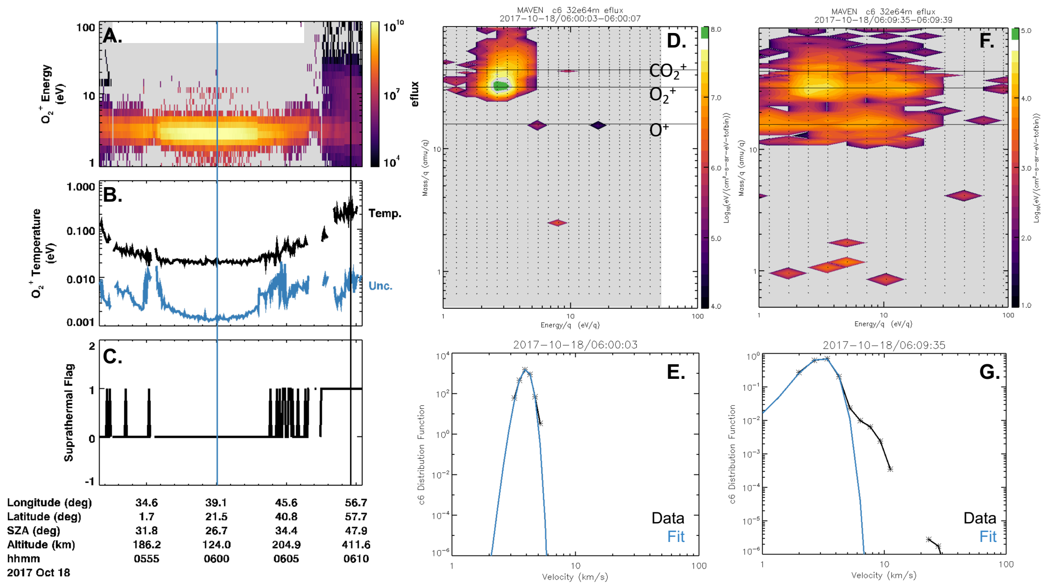

Figure 1. An example of STATIC data for one periapsis pass. Panel A: O_2^+ energy flux (eV/cm^2/s/steradian/eV). Panel B: O_2^+ temperature (black) and statistical uncertainty (blue). Panel C: A flag where 1 (0) indicates the presence (absence) of a suprathermal population. Vertical blue and black lines in panels A-C indicate the events shown in panels D/E and F/G, respectively. Panels D and F: Differential energy flux (color scale) vs energy and mass. Dotted lines show the locations of STATIC energy bins and shading shows the extent of the energy sweep. Panels E and G: Measured velocity distribution function (symbols with black lines) for O_2^+ with Maxwell-Boltzmann fits to the core (blue).

bins of 10° or 15°, as indicated in each figure, to investigate how O_2^+ distributions vary depending on these parameters. Given temperature ranges correspond to interquartile ranges of a group of binned measurements, not uncertainties in a particular measurement (typically ∼10% (Hanley et al., 2021)).

2.2 Identification of suprathermal ions

Below the exobase (∼180-200 km (Fox & Hać, 2009)), high collision rates should result in rapid thermalization with neutrals, so ion distribution functions are expected to be approximately Maxwellian. After correcting for spacecraft potential, we fit the core of each measured distribution with a drifting Maxwell-Boltzmann function. The fit is subtracted from the data, and the energy flux (eflux) in the residual suprathermal component is compared to the eflux contained in the best-fit Maxwell-Boltzmann function.

We define a significant amount of suprathermal eflux as >10% of the eflux in the Maxwellian fit.

An example of STATIC data collected during a periapsis pass is shown in Figure 1. The pass occurred during a Deep Dip, an orbit maneuver designed to sample the ionospheric peak and to approach the well-mixed region of the atmosphere. Periapsis is located near the center of Figure 1A-C. Figure 1A and B shows measured efluxes and temperatures for O_2^+ and Figure 1C shows a flag that indicates the presence of a significant suprathermal component. Shaded regions in Figure 1A, D, and F indicate different regions of energy space that STATIC sampled during different parts of the orbit. During the low-altitude segment, ion thermal velocities are much smaller than the spacecraft velocity, so that ions are beamed at the ram energy (2.7 eV for O_2^+); the energy sweep is subsequently restricted to energies<50 eV. At higher altitudes (>∼300 km), where suprathermal components may appear, the instrument sweeps up to 500 eV. A distribution observed near periapsis is shown in Figure 1D and E. In the collisional region around periapsis, a drifting Maxwellian contains nearly all measured eflux (Panel E). Above the exobase, a suprathermal tail appears (Panel F,G) that increases the density above escape energy from 0 to 10/cc (∼20% of the total density).

3 Evolution of the distribution function with altitude

Using the fitting routine described in Section 2.2, we have separated distributions into three categories based on suprathermal eflux; the fraction of distributions in each category is shown as a function of altitude and SZA in Figure 2. The categories are:

- Maxwellian: The fit contains >90% of the eflux of the measured distribution (Figure 2A).
- Significant suprathermal component: The suprathermal eflux is between 10% and 100% of the eflux in the fit to the Maxwellian core (Figure 2B).
- Mostly suprathermal: The suprathermal eflux exceeds the eflux in the fit (Figure 2C).

O_2^+ distribution functions are dominated by the Maxwellian core at all SZAs below altitudes of 200 km, in agreement with predictions from photochemical theory (e.g. Fox & Hać, 2009) that the exobase region is located there and collisions quickly ther-

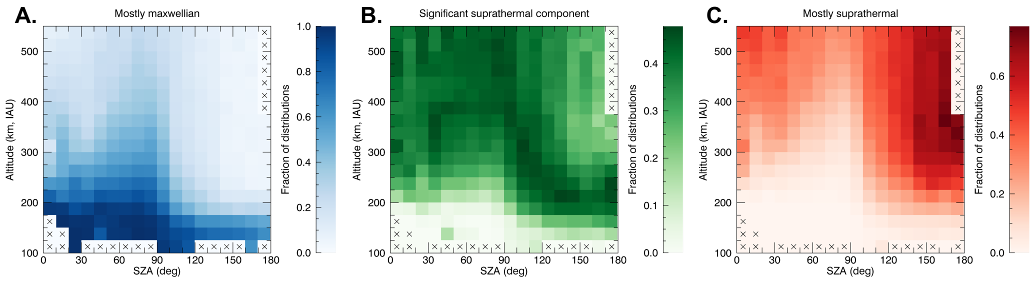

Figure 2. Occurrence rates for distribution functions classified as (A) mostly Maxwellian, (B) having a significant suprathermal component, or (C) mostly suprathermal as described in the text, sorted by solar zenith angle (SZA) and altitude. Each colorbar has a different upper bound. Xs indicate bins with no data.

malize ions at lower altitudes. The exact location of the exobase varies by tens of kilometers depending on external drivers that are averaged over in this study, such as Martian season and solar conditions (Jakosky et al., 2017).

The transition from collision-dominated Maxwellian distributions to distributions with a significant suprathermal component occurs just above 200 km for all SZAs at Mars (Figure 2). Panel A shows that Maxwellian distributions dominate below ∼250 km on the dayside and below ∼175 km on the nightside, which is consistent with the variation of the exobase altitude with SZA (Jakosky et al., 2017). On the dayside, Maxwellians extend to higher altitudes a fraction of the time, which does not occur on the nightside. This difference is likely due to differences in magnetic topology between the day and night, but we defer discussion of magnetic topology to Section 5. In panel B, suprathermal components begin to appear above the exobase, consistent with energized ions becoming unable to thermalize due to decreasing ion-neutral collision rates. These suprathermal components are typically non-Maxwellian and appear at different energies and directions depending on their energization mechanisms. At high altitudes, non-thermal distributions dominate, especially on the night side (Panel C).

On the nightside, the transition occurs over a narrow altitude range. By 250 km, most distributions are suprathermal. The transition region occurs over a broader altitude range on the dayside, but most distributions are suprathermal by ∼400 km. It is important to note that we have not compared suprathermal ion energies to escape energy to quantify the fraction of ions that can actually escape; however, the region where suprathermal ions appear is important as this marks the region where energized ions can no longer thermalize with the main population. Future work will investigate the likelihood that suprathermal ions escape to space, as well as mechanisms leading to the development of the suprathermal component at different SZAs.

4 Diurnal variations in ion temperature

Figure 3 shows median ion temperatures for Maxwellian distributions as a function of altitude and SZA (line color). Ion temperatures are calculated assuming a dominant Maxwellian core using the method described by Hanley et al. (2021) for their case studies of temperature profiles. Separating distributions with significant suprathermal components before beginning a statistical analysis reduces systematic errors, which will be discussed in Section 6. Panel A shows data collected throughout the mission. In Panels B and E, solid (dashed) lines indicate data gathered outside (inside) crustal fields. These regions are defined the same way as by *Fowler et al. (2022)*: the crustal field region covers the area of Mars' surface defined by 135° < longitude < 225°, -80° < latitude < 0°, while the non-field region covers the area 225° < longitude < 315°, 0° < latitude < 80°. Some fluctuations in Figure 3B and E likely result from a comparatively smaller number of samples; however, the general trends are still clear.

Figure 3D,E shows the variability in ion temperatures measured on different orbits in the same SZA-altitude bins; that is, a measure of inter-orbit variability on orbits that are not required to be consecutive, the same definition used by *Fowler et al. (2022)* when analyzing ion density. Variability is calculated using the interquartile range of O_2^+ temperatures in each SZA-altitude bin.

In the collisional region below the exobase, the dayside neutral atmosphere is warmer than the nightside (Stone et al., 2018), so ions in the collisional region should also be warmer on the dayside. Hanley et al. (2021) first reported dayside ion temperatures significantly hotter than expected, suggesting that an important source of ion energy is missing from current photochemical theory. The same trend is observed using the entire MAVEN dataset in Figure 3. Below 180 km, temperatures decrease with increasing SZA. Near the subsolar point, the median temperature at MAVEN's nominal periapsis altitude of 150 km is 0.025 ± 0.003 eV, decreasing to 0.023 ± 0.005 eV near the terminator and 0.016 ± 0.008 eV near the antisolar point. Inter-orbit variability is as low as 15% on the dayside

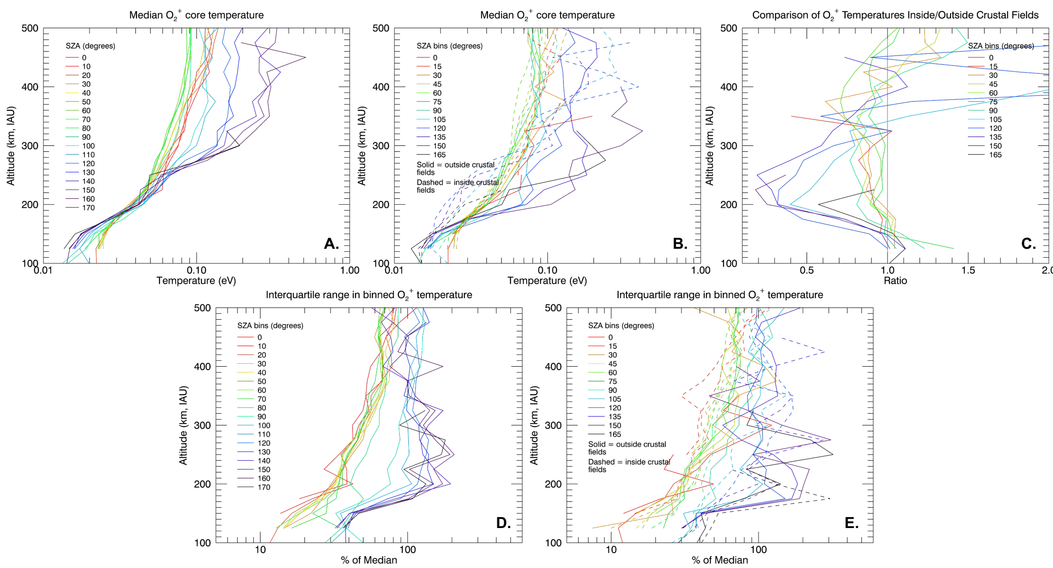

Figure 3. Panels A and B: Median temperatures for O_2^+ as a function of altitude and SZA. In panel B, solid and dashed lines indicate data collected away from and near crustal magnetic fields, respectively. Panel C: The ratio of median O_2^+ temperatures inside and outside crustal field regions. Panels D and E: Interquartile ranges of O_2^+ temperatures measured in each SZA-altitude bin, as a percentage of the median temperature in the same bin. Solid and dashed lines in Panel E have the same meaning as in Panel B.

and increases with SZA, up to 40% near midnight. Low variability on the dayside indicates highly repeatable structure there, while the higher variability on the nightside likely reflects variability in impact ionization, an important source of nightside plasma (Schunk & Nagy, 2009; Adams et al., 2018).

As ion-neutral collisional cooling becomes less efficient than ion heating towards the top of the exobase region, median temperatures begin to rise more quickly with altitude at all SZAs. This behavior is also observed at Earth as Coulomb collisions with electrons and electromagnetic waves provide heat sources for ions that increase in effectiveness with altitude (Schunk & Nagy, 2009).

Above 250 km, the coldest temperatures are found near the terminator, with subsolar temperatures $\sim$20% higher. In this altitude region, suprathermal components are more common at low SZAs than near the terminator: median temperatures are higher (Figure 3A) and Maxwellian distributions are rarer for SZAs $<60°$ (Figure 2). Between SZAs of 60° and 90°, median temperatures are coldest and most distributions are Maxwellian up to 400 km. Very few distributions are mostly suprathermal, although a suprathermal component does develop up to 50% of the time above 400 km (Figure 2). These hot ions are likely created near the top of the collisional atmosphere and do not collide enough times to thermalize with the neutral atmosphere. The magnetic geometry of the typical solar wind interaction with the planet may explain this behavior. Xu et al. (2019) showed that most field lines below 400 km near the terminator are draped interplanetary magnetic field lines or closed crustal loops. As closed field lines rotate towards the terminator and out of the solar wind dynamic pressure, they expand to higher altitudes, allowing thermalized ions to reach higher altitudes than at the subsolar point. Field lines open to the dayside, including field lines draped through the ionosphere, were the second most common topology observed below 400 km by Xu et al. (2019). Open and draped field lines crossing the terminator flare outwards, which also allows thermalized ions to reach higher altitudes in the terminator region.

On the nightside, median core temperatures are very high above 250 km (Figure 3A). For SZAs$>$100°, median temperatures increase with SZA and are hottest at midnight, reaching up to 0.195 $\pm$ 0.108 eV while dayside temperatures remain below 0.121 $\pm$ 0.083 eV. Variability increases with altitude, reaching 50-100% of the dayside median and 100-200% of the nightside median above 300 km ($\sim$5x more variability than at 180

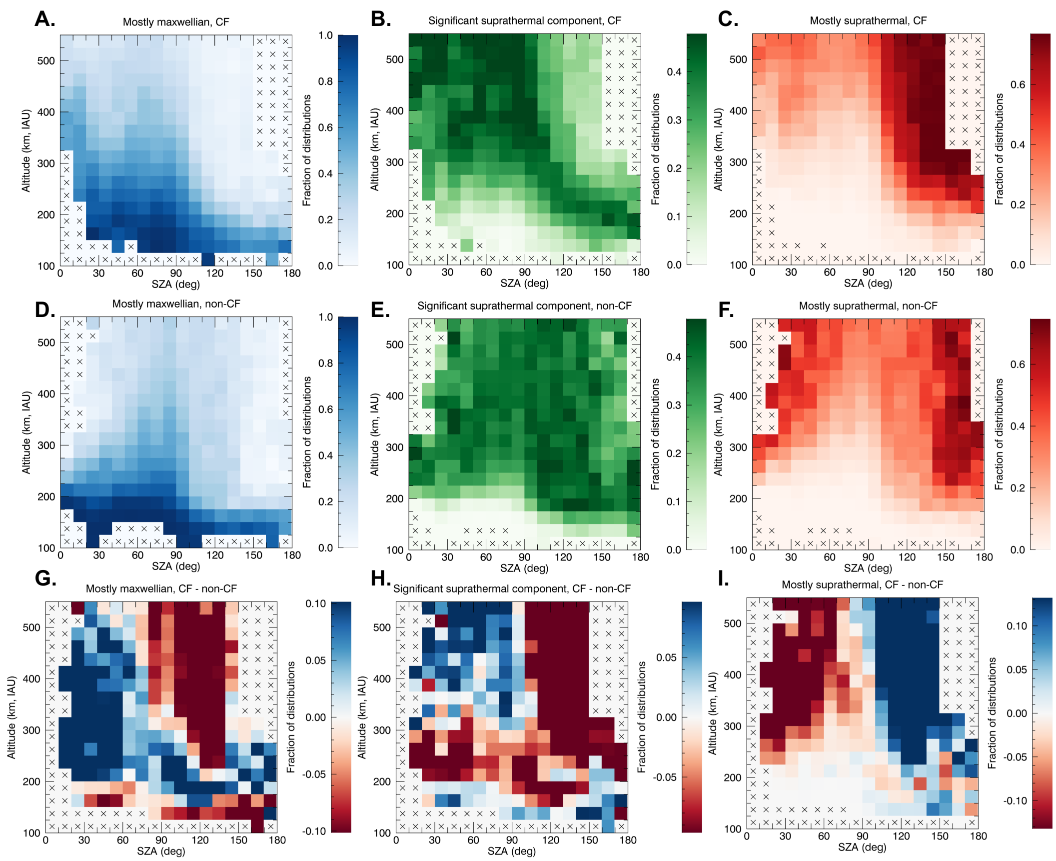

Figure 4. Panels A-C (D-F) are similar to Figure 2, representing data collected in the strong (weak) crustal field region defined in the text. Panels G-I are difference maps of panels A-F.

km, Figure 3D). Maxwellian distributions represent a very small fraction of measurements at these altitudes. Nearly all nightside distributions include suprathermal ions, indicating that ion-neutral collisional coupling is less important than energization mechanisms on the nightside.

5 Influence of crustal fields

Figure 3B and C compare O_2^+ core temperatures inside and outside regions characterized by strong crustal magnetism (Acuña et al., 1999). No clear trend is observed in the collisional region below 200 km. Between 200 and 350 km, core ion temperatures are significantly reduced in crustal field regions at all SZAs (Figure 3C). For SZAs of 15-30° (red-orange), crustal fields reduce temperatures by a factor of ∼10%, while nightside temperatures (dark blue) can be reduced by up to 90%.

Above the exobase, crustal fields appear to have significantly different effects on distribution functions at different SZAs. Figure 4 shows the fraction of distribution functions categorized as mostly Maxwellian, significantly suprathermal, or mostly suprathermal in the strong and weak crustal field regions. On the dayside, crustal fields appear to shield ionospheric O_2^+ from being heated and accelerated by the solar wind interaction: inter-orbit variability is reduced inside crustal fields (Figure 3E). For SZAs of 15-30° (red-orange), variability is reduced from 100% to 40% at 300 km in the strong field region. Also, the fraction of distributions that are Maxwellian is larger and extends to higher altitudes inside the strong field region (Figure 4A,D,G). For example, 70% of distributions are Maxwellian between 250 km and 275 km altitude for SZAs $< 90°$ in crustal field regions, compared to only 40% of distributions away from crustal fields. Suprathermal components appear at lower altitudes in weak field regions: for SZAs between 30° and 40°, 20% of distributions at 200 km have a suprathermal component, which does not occur until 250 km in the strong field region. The geometry of the crustal magnetic fields is critical in allowing thermalized ions access to higher altitudes than horizontal draped fields. In Figure 4G-I, suprathermal ions are observed less frequently in strong field regions all across the dayside, where crustal fields appear to protect planetary plasma from heating and acceleration.

Near the terminator between SZAs of 90° and 120° and altitudes of 150 and 300 km, Maxwellian core temperatures are colder (Figure 3C) and more distributions are mostly Maxwellian (Figure 4G) inside crustal field regions. The transition from cold to hot core temperatures is more gradual and extends to higher altitudes in crustal field regions near the terminator (Figure 3B). The transition from cold to hot ions occurs at lower altitudes at higher SZAs. Together, these observations imply that thermalized dayside plasma is trapped inside closed crustal fields as they rotate past the terminator. This interpretation supports previous results (e.g. Adams et al., 2018) that transport across the terminator is an important source of plasma at these SZAs.

In contrast to the dayside, the fraction of Maxwellian distributions above 300 km inside strong crustal fields is reduced for SZAs$>100°$ (Figure 4G). The increased incidence of suprathermal ions in crustal field regions suggests that crustal fields create conditions that enhance the efficiency of nightside ion energization at collisionless altitudes. Nightside thermal ions that do persist to high altitudes remain colder inside crustal fields: median core temperatures are reduced between 200 and 350 km (Figure 3C). This can be understood using magnetic topology. Weber et al. (2017) showed that open topologies dominate on the nightside above 180 km for magnetic field strengths < 10 nT, while closed topologies dominate up to 500 km in stronger fields. Particle precipitation down open field lines in weak field regions can lead to higher temperatures there, and thus an apparent reduction in temperature in strong field regions. Of the closed topologies seen in strong fields, plasma voids become less common above $\sim$300 km, giving way to trapped electron distributions. These transitions in topology, indicating regions of increasing efficiency of energization of planetary plasma, roughly coincide with the transitions from cold to hot nightside ions seen in Figure 3B. Again, magnetic topology is key for understanding trends in ion energization.

Above 350 km, the effect of crustal fields on core temperatures is less clear. The large fluctuations in Figure 3C make sense in the context of Figure 4A and D, which show that only a small fraction of distribution functions are Maxwellian above 350 km, and many bins have no data.

6 Sources of measurement bias

Care must be taken when interpreting ion temperatures measured above the exobase region, where suprathermal components appear in measured ion distribution functions. If multiple populations are present at different energies, or the eflux in the suprathermal portion of the distribution is significant compared to the eflux of the thermalized core, then the meaning of temperatures calculated assuming a dominant Maxwellian core becomes unclear. Data in Figure 3 are restricted to Maxwellian distributions so that the meaning of the calculated temperature is clear. However, restricting the data to Maxwellian distributions means that the temperatures reported here should be treated as a lower limit if used to calculate the amount of energy or pressure carried by the ions. Even a small fraction of suprathermal ions can represent a significant amount of energy compared to the cold core.

The most significant source of uncertainty in long-term statistical studies of STATIC data is the instrument's finite FOV. STATIC's FOV covers 360°x90°, not the entire sky, meaning that the peak of the distribution function may lie outside the FOV and lead to an inaccurate estimate of the temperature and/or errors in categorizing the distribution function. At low altitudes when the spacecraft travels supersonically, all the ions enter as a narrow beam centered on the ram direction, meaning it is straightforward to remove data collected when the instrument is mis-pointed and misses the beam, such as during orbits when the spacecraft communicates with Earth. At higher altitudes (>∼200 km) where distributions are broader, ion flow speeds can exceed the spacecraft speed, and the spacecraft can block a portion of the FOV from which ions might enter, determining whether the peak of the distribution is in the FOV is very difficult to automate. We have used the quality flag described by *Fowler et al., 2022* in order to remove data collected with incorrect pointing at low altitudes. FOV errors can be identified by manually inspecting the individual measurements made every 4 s, but this is unfeasible for a statistical study. We report median values and interquartile ranges rather than averages and standard deviations, which can be influenced by outliers, in an attempt to minimize the effect of FOV errors on altitude profiles.

Uncertainty in the categorization of distribution functions may also result from the fitting procedure. Entirely non-Maxwellian distribution functions are not represented in Figures 2 and 4. It is nearly always possible to fit a Maxwellian to a distribution function with one clear peak, and we make no test of goodness-of-fit beyond comparing measured and fitted efluxes as described in Section 2.2. However, for distribution functions that are doubly peaked or lack a clear peak, separating eflux into thermal and suprathermal components is impossible. Entirely non-Maxwellian distribution functions are a small fraction of the dataset (<1% below 500 km) and are almost never observed below the exobase. We thus expect uncertainties in the percentages of distributions in each category reported in Figures 2 and 4 to be on the order of a few percent. The smooth transitions between categories provide confidence that our qualitative description of ion behavior is correct.

Some of the variability in Figure 3 is a result of combining data measured in different Mars seasons, solar conditions, and magnetic topologies. A future study will investigate how solar drivers (e.g. dynamic pressure, interplanetary magnetic field direction) affect O_2^+ temperatures and distribution functions.

7 Summary

We present a statistical investigation of O_2^+ distribution functions measured in Mars' ionosphere with MAVEN-STATIC. Drifting Maxwell-Boltzmann functions are fitted to measured distributions in order to separate energized and thermalized distributions. The fraction of distributions categorized as Maxwellian, having a significant suprathermal component, and mostly suprathermal are presented as a function of SZA and altitude. Median temperatures for Maxwellian distributions as a function of SZA and altitude, as well as inside and outside regions of strong crustal magnetism, are also presented.

Ions are mostly Maxwellian below the exobase, in agreement with photochemical theory as collisions with neutrals are expected to rapidly thermalize the distributions. Above the exobase, ions are coldest near the terminator and hottest on the nightside; median ion temperatures increase with altitude, e.g. from 0.06 eV at 250 km to 0.3 eV at 400 km on the nightside. Cold, thermalized ions reach higher altitudes near the terminator due to magnetic field geometry. Magnetic field lines tend to flare outward while approaching the terminator, allowing cold plasma to reach higher altitudes.

Crustal fields appear to significantly reduce the presence of suprathermal ions on the dayside, likely by shielding planetary plasma from heating and acceleration mechanisms, while enhancing ion energization on the nightside. Between 200 and 350 km, core ion temperatures are significantly reduced in crustal field regions, particularly on the nightside.

Knowledge of where ion distributions transition from Maxwellian (driven by photochemistry and collisions) to suprathermal (driven by electromagnetic forces and transport) is a crucial first step in understanding the processes that control how ions at Mars are energized and can escape to space.

Acknowledgments

Data from MAVEN-STATIC are available at NASA's Planetary Data Center (https://pds-ppi.igpp.ucla.edu/search/view/?f=yes&id=pds://PPI/maven.static.c). This work was supported by NASA's Future Investigators in Earth and Space Science and Technology (Grant #80NSSC20K1388).

References

Acuña, M. H., Connerney, J. E., Ness, N. F., Lin, R. P., Mitchell, D., Carlson, C. W., ... Cloutier, P. (1999). Global distribution of crustal magnetization discovered by the Mars Global Surveyor MAG/ER experiment. *Science*, *284* (5415), 790–793. doi: 10.1126/science.284.5415.790

Adams, D., Xu, S., Mitchell, D. L., Lillis, R. L., Fillingim, M., Andersson, L., ... Mazelle, C. (2018). Using Magnetic Topology to Probe the Sources of Mars' Nightside Ionosphere. *Geophysical Research Letters*, *45* (22), 12,190–12,197. doi: 10.1029/2018GL080629

Akbari, H., Andersson, L., Peterson, W. K., Espley, J., Benna, M., & Ergun, R. (2019). Ambipolar Electric Field in the Martian Ionosphere: MAVEN Measurements. *Journal of Geophysical Research: Space Physics*, *124* (6), 4518–4524. doi: 10.1029/2018JA026325

Chaffin, M., Deighan, J., Schneider, N. M., & Stewart, A. I. F. (2017). Elevated atmospheric escape of atomic hydrogen from Mars induced by high-altitude water. *Nature Geoscience*, *10*, 174–178. doi: 10.1038/NGEO2887

Collinson, G., Wilson III, L. B., Omidi, N., Sibeck, D., Espley, J., Fowler, C. M., ... Jakosky, B. (2018). Solar Wind Induced Waves in the Skies of Mars: Ionospheric Compression, Energization, and Escape Resulting From the Impact of Ultralow Frequency Magnetosonic Waves Generated Upstream of the Martian Bow Shock. *Journal of Geophysical Research: Space Physics*, *123*, 7241–7256. doi: 10.1029/2018JA025414

Ergun, R. E., Andersson, L., Peterson, W. K., Brain, D., Delory, G. T., Mitchell, D. L., ... Yau, A. W. (2006). Role of plasma waves in Mars' atmospheric loss. *Geophysical Research Letters*, *33* (14), 3–7. doi: 10.1029/2006GL025785

Ergun, R. E., Andersson, L. A., Fowler, C. M., Woodson, A. K., Weber, T. D., Delory, G. T., ... Jakosky, B. M. (2016). Enhanced O2+ loss at Mars due to an ambipolar electric field from electron heating. *Journal of Geophysical Research: Space Physics*, *121*, 4668–4678. doi: 10.1002/2016JA022349.Received

Fowler, C. M., Andersson, L., Ergun, R. E., Harada, Y., Hara, T., Collinson, G., ... Jakosky, B. M. (2018). MAVEN Observations of Solar Wind-Driven Magnetosonic Waves Heating the Martian Dayside Ionosphere. *Journal of Geophysical Research: Space Physics*, *123*, 4129–4149. doi: 10.1029/2018JA025208

Fowler, C. M., Hanley, K. G., McFadden, J. P., Chaston, C. C., Bonnell, J. W., Halekas, J. S., ... Lillis, R. J. (2021). MAVEN Observations of Low Frequency Steepened Magnetosonic Waves and Associated Heating of the Martian Nightside Ionosphere. *Journal of Geophysical Research: Space Physics*, *126* (e2021JA029615). doi: 10.1029/2021JA029615

Fox, J. L., & Hać, A. B. (2009). Photochemical escape of oxygen from Mars: A comparison of the exobase approximation to a Monte Carlo method. *Icarus*, *204* (2), 527–544. doi: 10.1016/j.icarus.2009.07.005

Hanley, K. G., Mcfadden, J. P., Mitchell, D. L., Fowler, C. M., Stone, S. W., Yelle, R. V., … Jakosky, B. M. (2021). In Situ Measurements of Thermal Ion Temperature in the Martian Ionosphere. *Journal of Geophysical Research: Space Physics*, *126* (12). doi: 10.1029/2021JA029531

Jakosky, B. M., Brain, D., Chaffin, M., Curry, S., Deighan, J., Grebowsky, J., … Zurek, R. (2018). Loss of the Martian atmosphere to space: Present-day loss rates determined from MAVEN observations and integrated loss through time. *Icarus*, *315* (June), 146–157. doi: 10.1016/j.icarus.2018.05.030

Jakosky, B. M., Lin, R. P., Grebowsky, J. M., Luhmann, J. G., Mitchell, D. F., Beutelschies, G., … Zurek, R. (2015). The Mars Atmosphere and Volatile EvolutioN (MAVEN) mission. *Space Science Reviews*, *195* (1-4), 3–48. doi: 10.1007/s11214-015-0139-x

Jakosky, B. M., Slipski, M., Benna, M., Mahaffy, P., Elrod, M., Yelle, R., … Alsaeed, N. (2017). Mars ' atmospheric history derived from upper-atmosphere measurements of 38 Ar/ 36 Ar. *Science*, *355*, 1408–1410.

Lillis, R. J., Deighan, J., Fox, J. L., Bougher, S. W., Lee, Y., Combi, M. R., … Chaufray, J.-y. (2017). Photochemical escape of oxygen from Mars: First results from MAVEN in situ data. *Journal of Geophysical Research: Space Physics*, *122*, 3815–3836. doi: 10.1002/2016JA023525

Lundin, R., Zakharovt, A., Pellinen, R., Borg, H., Hultqvist, B., Pissarenko, N., … Koskinen, H. (1989). First measurements of the ionospheric plasma escape from Mars. *Nature*, *341*, 609–612.

McFadden, J. P., Kortmann, O., Curtis, D., Dalton, G., Johnson, G., Abiad, R., … Jakosky, B. (2015). MAVEN SupraThermal And Thermal Ion Compostion (STATIC) instrument. *Space Science Reviews*, *195* (1-4), 199–256. doi: 10.1007/s11214-015-0175-6

Ramstad, R., Barabash, S., Futaana, Y., Nilsson, H., & Holmström, M. (2018). Ion Escape From Mars Through Time: An Extrapolation of Atmospheric Loss Based on 10 Years of Mars Express Measurements. *Journal of Geophysical*

Research: Planets, *123*, 3051–3060. doi: 10.1029/2018JE005727

Schunk, R. W., & Nagy, A. F. (2009). *Ionospheres* (2nd ed.; J. T. Houghton, M. J. Rycroft, & A. J. Dessler, Eds.). Cambridge, United Kingdom: Cambridge University Press.

Slipski, M., Jakosky, B. M., Benna, M., Elrod, M., Mahaffy, P., Kass, D., … Yelle, R. (2018). Variability of Martian Turbopause Altitudes. *Journal of Geophysical Research: Planets*, *123*, 2939–2957. doi: 10.1029/2018JE005704

Stone, S. W., Yelle, R. V., Benna, M., Elrod, M. K., & Mahaffy, P. R. (2018). Thermal Structure of the Martian Upper Atmosphere from MAVEN NGIMS. *Journal of Geophysical Research: Planets*, *123*(11), 2842–2867. doi: 10.1029/2018JE005559

Weber, T., Brain, D., Mitchell, D., Xu, S., Connerney, J., Halekas, J., & Al, W. E. T. (2017). Characterization of Low-Altitude Nightside Martian Pitch Angle Distributions. *Journal of Geophysical Research: Space Physics*, *122*, 9777–9789. doi: 10.1002/2017JA024491

Xu, S., Mitchell, D. L., McFadden, J. P., Collinson, G., Harada, Y., Lillis, R., … Connerney, J. E. (2018). Field-Aligned Potentials at Mars From MAVEN Observations. *Geophysical Research Letters*, *45*(19), 10,119–10,127. doi: 10.1029/2018GL080136

Xu, S., Weber, T., Mitchell, D. L., Brain, D. A., Mazelle, C., Dibraccio, G. A., & Espley, J. (2019). A Technique to Infer Magnetic Topology at Mars and Its Application to the Terminator Region. *Journal of Geophysical Research: Space Physics*, *124*, 1823–1842. doi: 10.1029/2018JA026366